Soft Matter

PAPER

View Article Online
View Journal | View Issue

Cite this: *Soft Matter*, 2014, **10**, 5945

Hydrodynamic effects of the tip movement on surface nanobubbles: a combined tapping mode, lift mode and force volume mode AFM study

Wiktoria Walczyk,† Nicole Hain† and Holger Schönherr*

Received 10th May 2014
Accepted 18th June 2014

DOI: 10.1039/c4sm01024h

www.rsc.org/softmatter

We report on an Atomic Force Microscopy (AFM) study of AFM tip-nanobubble interactions in experiments conducted on argon surface nanobubbles on HOPG (highly oriented pyrolytic graphite) in water in tapping mode, lift mode and Force Volume (FV) mode AFM. By subsequent data acquisition on the same nanobubbles in these three different AFM modes, we could directly compare the effect of different tip-sample interactions. The tip-bubble interaction strength was found to depend on the vertical and horizontal position of the tip on the bubble with respect to the bubble center. The interaction forces measured experimentally were in good agreement with the forces calculated using the dynamic interaction model. The strength of the hydrodynamic effect was also found to depend on the direction of the tip movement. It was more pronounced in the FV mode, in which the tip approaches the bubble from the top, than in the lift mode, in which the tip approaches the bubble from the side. This result suggests that the direction of tip movement influences the bubble deformation. The effect should be taken into account when nanobubbles are analysed by AFM in various scanning modes.

1 Introduction

Surface nanobubbles that appear on surfaces immersed in water are responsible for the attraction between hydrophobic surfaces in water,[1–3] rupture of thin liquid films,[4,5] and hydrodynamic slip.[6] They play a role in immersion lithography,[7] froth-flotation,[8] and are a useful tool for cleaning surfaces fouled with proteins or nanoparticles.[9,10] Furthermore surface nanobubbles have been studied by various techniques including Atomic Force Microscopy (AFM),[11–13] neutron reflectivity,[14] attenuated total internal reflection Fourier transform infrared (FTIR) spectroscopy,[15] rapid cryofixation,[16] quartz crystal microbalance,[17] X-ray reflectivity,[18,19] synchrotron-based scanning transmission soft X-ray microscopy (STXM),[20] interference microscopy,[21] and total internal reflection fluorescence microscopy.[22,23]

Surface nanobubbles were found to be very soft and deformable. Their stiffness is comparable with the surface tension of water.[24,25] Based on their shape measured from AFM images, the estimated Laplace pressure exceeds the atmospheric pressure significantly, which should lead to their rapid dissolution. However, experimental observations confirmed that surface nanobubbles are stable for long periods of time.[26,27] Importantly, the internal pressure is calculated from the *apparent* nanobubble size and profile, which is extremely flat with nanoscopic contact angles higher than the macroscopic ones.[28–30] The unusual stability and high nanoscopic contact angles observed are issues that need to be addressed by the various theories on surface nanobubbles. These theories emphasize the role of contamination,[27,31,32] the substrate and pinning of the three phase contact line,[33–35] gas exchange between the bubble interior and surrounding liquid,[36–40] and the presence of surface charges.[41]

An accurate determination of the bubble size and shape is therefore critical. Practically all data in this respect has been derived from AFM experiments. However, it has been shown that AFM imaging may lead to several artefacts and complex sample deformation[42] and that the shape of nanobubbles in AFM height images may not reflect the real bubble size and shape.[24,43] It is in general difficult to extract the actual shape of nanobubbles from a single AFM image because each image combines the information about the sample, the AFM tip and a number of parameters related to the scanning procedure. So far, it has been shown that the apparent bubble height and radius of curvature of surface nanobubbles in AFM height images depend on the tip shape,[30] the amplitude of the cantilever oscillations and the amplitude setpoint ratio in TM (Tapping Mode) AFM[43–46] and on the peak force in Peak Force Tapping AFM.[25,47,48]

Moreover, the choice of the AFM tip *i.e.* size, material and cleanness are crucial and can entirely change the result of AFM experiments on surface nanobubbles.[24] Only if the tip is hydrophilic, the interaction between the tip and the bubble is

Physical Chemistry I, University of Siegen, Department of Chemistry and Biology, Adolf-Reichwein-Str. 2, 57076 Siegen, Germany. E-mail: schoenherr@chemie.uni-siegen.de

† These authors contributed equally.

ruled by hydrodynamic forces. In this case a thin film of water remains between the tip and the bubble surfaces at all stages of (intermittent) contact. Pressing the tip against the bubble surface causes its deformation and a squeezing of the liquid film that gives rise to the dynamic forces acting on the tip. During the AFM measurement, the hydrophilic tip "slides" over the bubble surface and the bubble continuously adapts its shape to the shape of the tip. By contrast, a contaminated or hydrophobic tip attracts the bubble surface, penetrates the bubble during the contact and may even drag the bubble over the sample. In extreme cases, it may move nanobubbles away from the scanning area. Therefore, hydrophobic tips are not suitable to interrogate nanobubbles.

In addition, low force conditions must be employed, which demand a sharp, hydrophilic tip and a cantilever with a small spring constant as well as small amplitudes of the cantilever oscillations and high amplitude setpoint ratios in TM. During the measurement the tip always distorts the bubble surface and as a result a distorted bubble shape is detected in the height image. This effect is independent from the scanning mode. Hence in order to extract information about the actual bubble shape and size from AFM images, it is necessary (i) to know which parameters influence the bubble appearance in the experiment and (ii) to estimate their individual contributions to the particular image. Importantly, one should not directly compare images of nanobubbles acquired under entirely different (or unknown) scanning conditions.

While we can compare the data obtained using different experimental conditions in a particular scanning mode, it remains more difficult to compare results obtained in different AFM modes. Most of the experiments were carried out in TM,[11,28,36–40,49] CM (Contact Mode),[12,13,50,51] Peak Force Mode,[25,47,48] FM (Frequency Modulation) mode,[47,52] force spectroscopy (Force–Volume mode or FV mode),[53] non-contact mode,[35] and lift mode AFM.[49] All these modes have their own specific methods of data acquisition, scanning procedures and parameters involved.

In order to shed light on the response of nanobubbles to the scanning tip in different AFM modes, we conducted an experiment on surface nanobubbles in three different AFM imaging modes: TM, lift mode and FV mode AFM. In particular, we discuss the tip-bubble interactions and nanobubble deformation under different AFM imaging conditions for individual bubbles.

2 Experimental

Sample preparation

In the experiments freshly cleaved highly oriented pyrolytic graphite (HOPG) (Veeco, grade ZYH) with a water contact angle of $63 \pm 2^{\circ}$ was used. The static contact angle was measured with the sessile drop method with an OCA 15plus instrument (Data Physics Instruments GmbH, Filderstadt, Germany) using Milli-Q water obtained from a Millipore Direct Q8 system (Millipore, Schwalbach, Germany) with resistivity of 18.0 MΩ cm^{-1}. Nanobubbles were measured in Argon saturated Milli-Q water, which was prepared as reported earlier.[24]

Atomic force microscopy

The AFM measurements were carried out on a MultiMode IIIa AFM instrument (Bruker/Veeco, Santa Barbara, California) with a vertical engage E-scanner and NanoScope version 3.10 software (Bruker/Veeco AXS, Santa Barbara, CA). V-shaped MLTC Si_3N_4 cantilevers (Bruker AXS, Camarillo, CA) with a spring constant of $k_{cant} = 0.05 \pm 0.005$ N m^{-1} was used. The spring constant was independently calibrated on an Asylum Research MFP-3D Bio (Asylum Research, Santa Barbara, California). The cantilever was cleaned prior to the measurements for 60 s by oxygen plasma (Plasma PrepIITM, SPI Supplies, West Chester, USA).

In all experiments, a closed liquid cell configuration was used. First, the liquid cell, the O-ring (fluorosilicone rubber) and the silicone inlet and outlet tubes were rinsed with Milli-Q water and with ethanol (99.9%, Merck KGaA, Darmstadt, Germany) and dried in a stream of nitrogen. Next, the liquid cell was assembled and the cantilever was inserted. Subsequently, a 1 mL sterile syringe (Braun, Injekt-F 0.01-1mL/luer Solo) cleaned with Milli-Q water was filled with the Ar saturated water and connected to the inlet tube. No needle was used. Immediately afterwards the water was injected in the liquid cell until the cantilever was immersed and the O-ring was filled. Then the liquid cell was put on the sample, the O-ring was brought in contact with the sample, 0.6 mL of water was passed through the liquid cell and after that, the inlet and outlet were closed. We stress that *no* liquid exchange procedure was performed and the HOPG surface did not have contact with ethanol at any stage of the experiment. Before the start of the AFM measurement, the system was left to equilibrate for 30 min. The nanobubbles were then scanned first in TM AFM and subsequently in lift mode and in force volume mode AFM without changing the cantilever and the tip or replacing the liquid.

The TM deflection data reported in this study refer to the root mean square (rms) averaged cantilever deflection (TM deflection) that can be recorded in TM AFM as a separate channel in addition to conventional height (vertical piezo displacement to keep a constant amplitude), amplitude and phase. This deflection signal (also in deflection–displacement curves) is low-pass filtered to eliminate the high-frequency Tapping Mode oscillation. For technical details, see, *e.g.* Veeco MultiMode SPM Instruction Manual RevB Nanoscope5 pp.199–200.

Lift mode

Deflection images were acquired in the interleave scan in the linear lift mode. Each line was first scanned in the forward direction (trace) in TM with the following settings: drive frequency 29.6 kHz, free amplitude 46 nm and setpoint ratio 94%. After completing the line, the tip was lifted 200 nm in order to pull the tip off the surface. Next, the cantilever oscillation was switched off, the tip was lowered to the requested lift height and the line was rescanned at fixed lift height above the start point of the line in the backward direction (retrace) in the lift mode, *i.e.* the lift mode scan did not follow the contour of the line recorded in TM during the trace scan. All AFM

deflection images shown here are retrace images. Raw height and deflection images were processed using a 1st order planefit and a 0th order flattening (with nanobubbles excluded). The data analysis was performed with Nanoscope software version 3.10. The bubble size in TM height images was measured using the spherical cap fitting without applying a correction for the tip size.[30]

Force volume mode (FV AFM)

In this mode, the tip was lowered and retracted at each point of the selected area of the sample and the interaction forces during approach and retraction were measured. The resolution of the grid of positions imaged was limited to 32 × 32 pixels.[2] The cantilever oscillation was switched off. The tip approach velocity was set to 1.02 μm s^{-1} and the force curve resolution to 512 points per single force curve cycle. The raw deflection–distance curves were transformed into deflection-separation curves.[54] The vertical position of the tip above the substrate is represented in the plots by the tip-sample separation distance. The deflection was recalculated into force by multiplying the measured deflection value with the cantilever stiffness.

3 Results

In the experiments, argon surface nanobubbles were investigated in TM, lift mode and FV AFM. Fig. 1 shows the principles of data acquisition and details of the tip operation in scanning in the three considered imaging modes. In TM AFM, the cantilever is oscillated near resonance and the oscillating tip moves slowly horizontally along the scan line following the sample surface. In the lift mode, the tip moves horizontally at the fixed separation distance (lift height) to the planar substrate, while the deflection of the cantilever is recorded. In the FV mode, the tip is moved for each pixel vertically at a fixed position on the sample in and out of contact with the surface.

First, a 5 × 5 μm^2 area of HOPG containing nanobubbles was scanned in TM AFM. The acquired height and deflection images are shown in Fig. 2a. Apart from the atomic steps and surface nanobubbles, the graphite surface was flat and homogeneous without visible micropancakes[28] or contamination. The five largest bubbles, marked in the image with numbers, had apparent heights between 10 and 15 nm, and apparent widths between 300 and 700 nm. In the TM deflection image acquired simultaneously with the height image, the color scale encodes

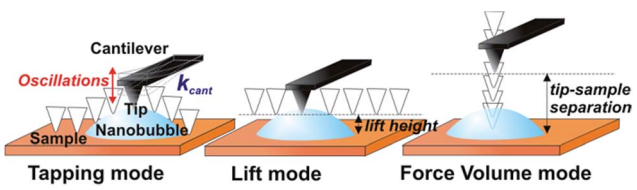

Fig. 1 Schemes of the movement of the AFM tip during scanning in the different AFM modes. In tapping mode and in lift mode the tip is moved horizontally along the scan line, whereas in the force volume mode the tip is moved pixel by pixel vertically at a fixed position on the sample.

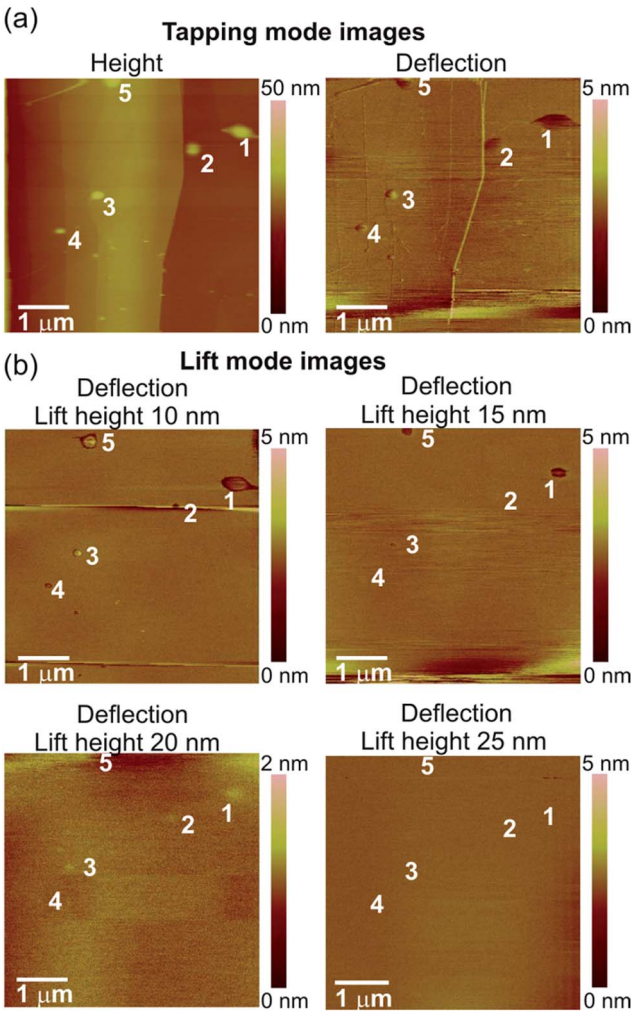

Fig. 2 (a) AFM TM height and deflection and (b) lift mode images (deflection of the cantilever at different lift heights between 10 and 25 nm) of surface nanobubbles on HOPG in water. The five largest nanobubbles are marked with numbers. The cross-sections of the bubble no. 1 are shown in Fig. 5.

the cantilever bending. The locations of the nanobubbles could be recognized as circular spots. Dark color marked the positions on the sample, where the cantilever bent more downwards, and bright color marked the positions, where the cantilever bent more upwards, as compared to its bending on the graphite surface. The bubbles in the TM deflection image and the corresponding bubbles in the TM height image had similar widths.

Next, the same area of the sample was rescanned in the lift mode. Each line of the image was scanned in TM mode on the way forward (from left to right), while on the way back (from right to left) the scanning was done with the cantilever lifted over the substrate at a certain lift height. It means that during the scanning of a single image, the tip was moved up and down repeatedly because of the continuous switching between TM and lift mode. During the lift mode data acquisition the deflection of the cantilever was measured as the tip was being moved horizontally over the sample. The lift height was increased for each image from 10 to 120 nm in 5–10 nm steps.

Four deflection images measured over the sample at lift heights of 10 nm, 15 nm, 20 nm and 25 nm are shown in Fig. 2b.

The lift mode deflection images were featureless over most of the scanned area of the sample. This means that there was no interaction between the tip and the graphite when the separation distance was larger than 10 nm. Surface nanobubbles were visible in the lift mode images as dark circular spots located at the positions that correspond to the positions of the bubbles identified in the TM height images. In the lift mode deflection image acquired at a lift height of 10 nm, the width of each bubble was slightly smaller than the apparent width of the footprint of the corresponding bubbles in the TM height image in Fig. 2a. Interestingly, although all five bubbles were visible in the lift mode deflection image, some appeared with dark contrast, while other appeared bright. As the lift height increased to 15 nm, the bubbles in the deflection image appeared dark and considerably smaller (bubbles 1, 3 and 5) or they disappeared from the image (bubbles 2 and 4). At a lift height of 20 nm, the bubbles were visible as slightly bright spots almost undistinguishable from the substrate (mind the different vertical color scales in Fig. 2b). Finally, at lift heights of 25 nm and larger the deflection images were featureless.

To explain the different deflection signals in the lift mode images, we have analysed force data acquired on the same bubbles in FV mode AFM. In addition, these force measurement also afforded information on the cantilever deflection on the bubble, but acquired in a different way than in the lift mode. In the FV experiment, the tip was lowered and retracted at several positions on the bubble, and the forces acting on the tip (deflection of the cantilever) at different tip-sample separation distances were measured. In the measurement, FV height image and FV slice image of the HOPG sample with the nanobubbles were acquired simultaneously. Both images are displayed in Fig. 3. The FV height image shows how much the AFM tip was moved in the vertical direction at each point of the sample in order to reach the requested maximum deflection threshold (always exceeding a nanobubble height). The FV slice image shows the magnitude of the cantilever deflection at a particular height over the substrate (here, comparable with the bubble height). The nanobubbles were visible only in the FV slice image. By comparing the sample features in the FV height image with the TM height image shown in Fig. 2a, the bubbles in the FV slice image could be identified. Bubble no. 1 is marked with a box. Exemplary force curves measured on this bubble are shown in Fig. 4. For clarity, only approach force curves are shown in the plots.

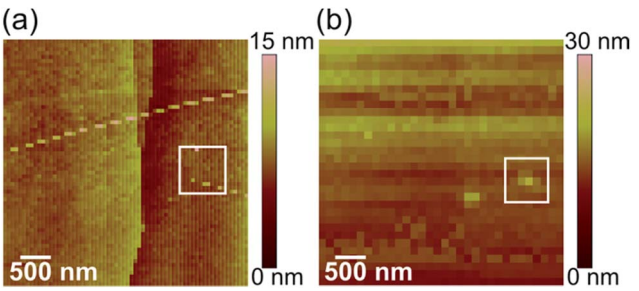

Fig. 3 (a) FV AFM height image and (b) FV AFM force slice image of HOPG with nanobubbles. Nanobubble no. 1 from Fig. 2 is marked with a box.

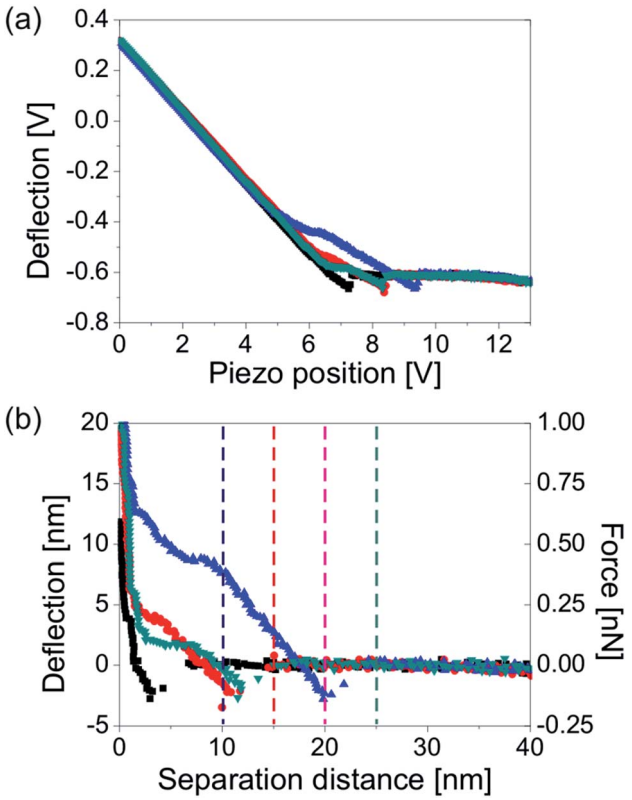

Fig. 4 (a) Unprocessed force–displacement and (b) force–distance curves acquired on nanobubble no. 1 from Fig. 2. The deflection measured at positions 10 nm, 15 nm, 20 nm and 25 nm (marked with four vertical lines) are plotted in Fig. 5b. The data were acquired with a cantilever with a spring constant $k_{cant} = 0.05$ N m^{-1}.

Since we know how the deflection of the cantilever changed with the tip-sample separation distance, we could extract the information on the deflection at a particular separation distance to the substrate. In Fig. 5, we directly compare the results of the lift mode and force measurements done on nanobubble no. 1 from Fig. 2. The graphs show the deflection signals measured at different tip-sample separation distances imposed on the bubble height profile. Three cross-sections of the bubble no. 1 are plotted. The first cross-section (open squares) shows the apparent shape of the bubble measured directly from the TM height image. The second cross-section (black solid squares) is the bubble profile corrected for non-ideal scanning conditions *i.e.* non-zero amplitude of the cantilever oscillations and amplitude setpoint ratio lower than 100%.[43] The corrected bubble height was estimated to be 17 nm. The third cross-section (solid squares – shown only in the plots in Fig. 5b) is the bubble profile reconstructed from the force–distance curves (the procedure is described further in this article). Because of the low spatial resolution of the FV measurement, the reconstructed profile only roughly resembles

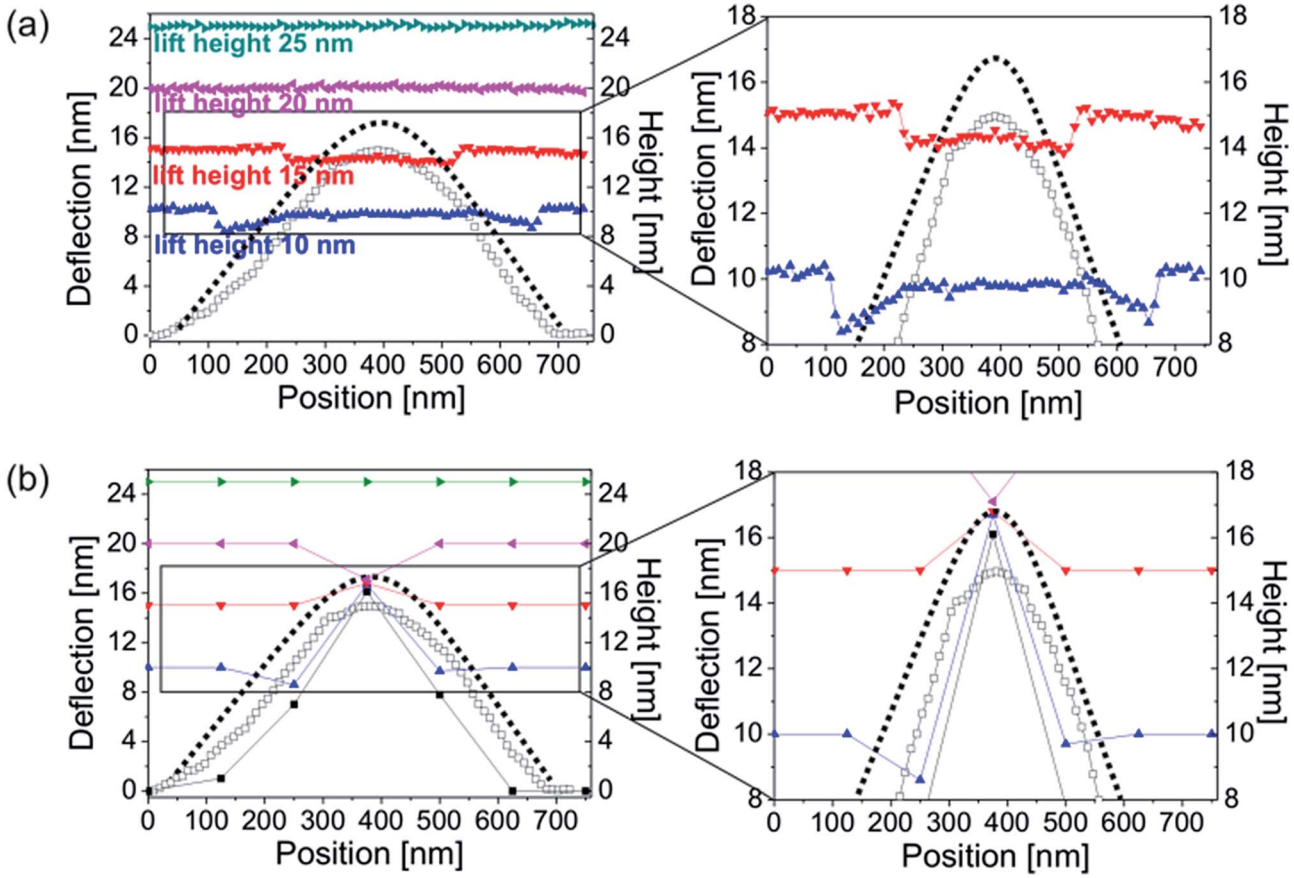

Fig. 5 Deflection of the AFM cantilever over bubble no. 1 from Fig. 2 (a) measured directly in lift mode scans at lift heights of 10 nm, 15 nm, 20 nm and 25 nm, and (b) measured from the approach force–distance curves acquired on the bubble in the FV mode at tip-sample separation distances of 10 nm, 15 nm, 20 nm and 25 nm. The apparent (black open squares) and corrected (black solid squares) bubble profiles measured from the TM AFM height image are compared to the profile estimated from the force–distance curves (black squares in panel b). The plots on the right hand side showing the bubble top are a magnification of the adequate part of the plots on the left hand side. The data were acquired with a cantilever with a spring constant $k_{cant} = 0.05$ N m^{-1}.

the spherical cap. Nevertheless, its height was similar to the height of the corrected TM profile.

The measured and calculated bubble profiles were used as a reference in order to show the deflection of the cantilever measured at different tip-sample separation distances. The deflections plotted in Fig. 5a were extracted from the lift mode images shown in Fig. 2b. The deflections plotted in Fig. 5b were measured from the force–distance curves acquired over the nanobubble at the separation distances of 10 nm, 15 nm, 20 nm and 25 nm, as marked with four vertical lines in the force plot in Fig. 4b. All plotted deflections were measured along a single scan line approximately over the bubble center.

For simplicity, in each case we assumed that the cantilever was in an unbent position and its deflection was zero, when it was far away from the bubble. However, in order to give a better overview of the experiment and the results, all cantilever deflections in Fig. 5 are plotted at the levels approximately equal to the actual separation to the substrate, where the tip end was located during the experiment. For example, zero cantilever deflection away from the bubble is plotted as equal to 10 nm, if it was measured at the lift height/tip-sample separation of 10 nm, and as equal to 15 nm if it was measured at the lift height/tip-sample separation of 15 nm, and so on. Consequently, all data points located below the initial deflection level indicate a downward bending of the cantilever at these positions, whereas data points located above this level indicate an upward bending. The values of TM deflection measured directly on the sample were not included in the plots.

In TM AFM in liquid, the cantilever always bends as soon as the tip interacts with the surface. However, because at the same time the cantilever is oscillated, the tip-bubble interaction conditions are different than in the other two imaging modes. For this reason, we cannot quantitatively compare the TM deflection signal with the results obtained in the other modes.

In the plots in Fig. 5, all deflections measured over the bubble at tip-sample separation distances smaller than or equal to the corrected local bubble height were non-zero. Regardless the direction of the tip movement – horizontal in the lift mode and vertical in the FV measurement, the cantilever started to bend when the tip approached the bubble, and remained bent

until the tip left the bubble. Interestingly, the spatial extent of non-zero deflection was slightly larger in the lift mode than in the FV mode.

Now, we will look in detail at the deflection of the cantilever at different tip-sample separation distances. In the lift mode, at lift heights of 10 nm and 15 nm the deflection measured on the bubble was smaller than the one measured on the substrate (*i.e.* the cantilever bent downwards). However, the deflection value varied at different positions over the bubble. This is clearly visible in the right plot in Fig. 5a that shows in detail the data points acquired at lift heights of 10 nm and 15 nm. It is clear that at a lift height of 10 nm, the downward deflection of the cantilever was the largest (~2 nm) near the rim just outside the bubble. When the tip interacted with the bubble, the deflection decreased in magnitude to ~0.5 nm and stayed approximately constant at all positions while traversing the bubble, until the tip reached the bubble rim and the deflection increased again to ~2 nm. A similar behavior of the cantilever could be observed at a lift height of 15 nm, however, the tip-bubble interaction was weaker so that the cantilever bent downward only by ~1 nm and this bending was nearly constant on all positions over the bubble – the data points formed an almost straight line in the plots in Fig. 5a. The deflection data for the lift heights of 20 nm and 25 nm were featureless.

If we look at the plots in Fig. 5b that show the cantilever deflection values over the same bubble measured from the force–distance curves, we observe a similar cantilever response to the bubble as measured in the lift mode. At a tip-sample separation distance of 10 nm, the deflection near the bubble rim was slightly decreased (bending down by ~1 nm) as compared to the deflection measured away from the bubble. In turn, near the bubble center, the measured deflection value was increased and the cantilever bent upwards by ~6 nm. A similar but weaker (~2 nm) upward bending of the cantilever near the bubble center was observed at a tip-sample separation distance of 15 nm. Unfortunately, we cannot discuss the changes in the cantilever deflection at different horizontal positions over the bubble because of the small spatial resolution of the FV measurement. At a tip-sample separation distance of 20 nm, a weak (~3 nm) downward bending of the cantilever on the bubble was observed in the FV mode, whereas no change in the deflection signal was measured over the bubble in the lift mode. Finally, the deflection data extracted from the force–distance curves was featureless at a separation of 25 nm to the substrate.

4 Discussion

The cantilever deflection signal measured on the nanobubbles varied depending on the tip-sample separation distance and the horizontal position of the tip over the bubbles, as shown in Fig. 2 and in Fig. 5.

In the experiment, the nanobubbles were visible in the lift mode deflection image, when the lift height was smaller than the unperturbed bubble heights. The statement is supported by the results shown in Fig. 2. Only the largest bubbles no. 1 and no. 5 shrank, but did not disappear in the lift mode deflection image acquired at a lift height of 15 nm. The corrected heights of these bubbles measured from the TM image were equal to 17 nm and 18 nm, respectively. Therefore they were both larger than the lift height level. The heights of the remaining bubbles no. 2, 3 and 4 were smaller and equal to ~12 nm. In addition, as shown in the plots in Fig. 5a, no tip-sample interaction was detected at separation distances larger than the bubble height.

If we assume that the nanobubble resembles a spherical cap, the shrinking of the circular spots representing the bubbles in the lift mode deflection images acquired at increased tip-sample separation distances might be a pure geometrical effect and approximately corresponds to a decrease in circumferences of the bubbles at increased heights above the HOPG. In other words, in the lift mode images done at different lift heights, we can see different horizontal "slices" of the bubbles. The data shown in the plots in Fig. 5 confirm this hypothesis. At small tip-sample separation distances the total horizontal distance, over which the tip interacted with the bubble, was larger than at increased separation distances, which is the consequence of different bubble widths at different distances to the substrate. These results explain not only why the bubbles shrank in the deflection images acquired at increased lift heights, but also why small bubbles disappeared from deflection images sooner than large bubbles.

If we decrease the lift height, the lateral size of the bubble in the deflection image will approach the bubble width measured from the TM height image. For zero lift height, the bubble width measured in the deflection image and in the TM height image should be equal. If we compare the TM height image shown in Fig. 2 with the TM deflection image (acquired directly on the sample), and with the lift mode deflection image (acquired at a lift height of 10 nm), we see that the bubbles have similar footprint widths in the TM height and deflection image, while they appear slightly smaller in the lift mode image (at 10 nm lift height). For example, for the bubble no. 1, the widths are 656 nm (TM height), 675 nm (TM deflection) and 607 nm (lift height 10 nm, lift mode deflection). The TM bubble width and the horizontal extent of the deflection signal measured at 10 nm lift height can also be seen in the plot in Fig. 5a. The observation that a single nanobubble displayed similar widths in various imaging channels or modes, was reported for Peak Force AFM experiments.[25,47,48]

Previously, the qualitative agreement between the results obtained in the FV mode and in lift mode AFM indicates that the variations in the deflection signal with the tip-sample separation distance were well reflected in the shapes of the force–distance curves. As shown in the exemplary force curves in Fig. 4b, the deflection of the cantilever on the bubble changed in the magnitude or/and the direction depending on the distance of the tip to the sample. We believe that this effect explains the switching between positive (upward bending) and negative (downward bending) deflection values observed in the deflection images in Fig. 2b acquired at different lift heights. In addition, because each change in the deflection sign from positive to negative values or *vice versa* required crossing the zero deflection point at a certain tip-sample separation distance, our results explain why sometimes nanobubbles did not appear in the deflection image acquired at small lift

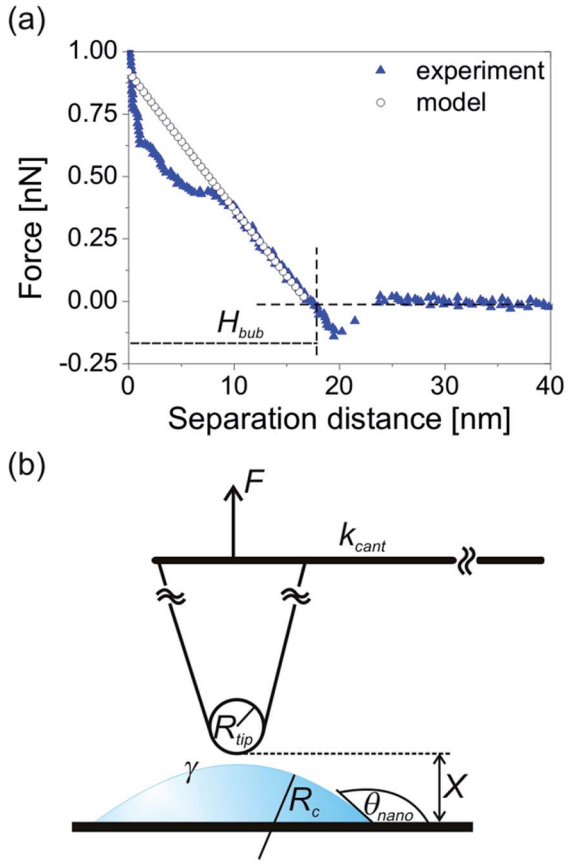

Fig. 6 (a) Approach force–distance curve acquired on the bubble no. 1 from Fig. 2 and forces calculated from the dynamic interaction model. The data were acquired and calculated with the cantilever with spring constant $k_{cant} = 0.05$ N m^{-1}. (b) A schematic diagram of AFM tip interacting with surface nanobubble. The parameters used in the dynamic interaction model are defined.

heights/tip-sample separations, and reappeared in the deflection image done for larger lift heights/separations. Finally, because force–distance curves acquired on bubbles of different vertical sizes have different shapes, our results also explain, why different bubbles appear as bright or dark in a single lift mode deflection image measured at a fixed tip-sample separation distance.

As already mentioned, the deflection data extracted from the force curves resembles the lift mode deflection data qualitatively. However, larger cantilever bending was detected in the force measurement, which suggests stronger tip-bubble interaction. The maximum deflection measured on the bubble in the force mode was as large as 6 nm (which corresponds to a repulsive force of 0.3 nN), whereas the maximum deflection measured in the lift mode did not exceed 2 nm (which corresponds to an attractive force of 0.1 nN). Taking into account that the same cantilever and tip was used in the whole course of the experiments, this result is puzzling. The cantilever seemed to be less sensitive in the lift mode than in the force measurement. The lack of precise control of the tip-sample separation distance due to the open feedback loop system used in the lift mode cannot account for the observed discrepancy.

In order to explain the difference in the interaction strength, we need to focus on the tip-bubble interaction. Force–distance curves acquired on the bubble are a valuable source of information. First, from the course of the force curve we could measure the unperturbed nanobubble height H_{bub}.[24] As shown in the example in Fig. 6a, for each force–distance curve acquired on the bubble, the local unperturbed bubble height H_{bub} is equal to the separation distance of the zero-deflection crossing point that follows the jump-in event. The height extracted from the force curves measured near the bubble center will be larger than the height extracted from the force curves measured near the bubble edge. This method was used to reconstruct the bubble profile plotted in Fig. 5b (black squares).

Next, we apply the dynamic interaction model to the force curve measured approximately at the bubble center.[55–57] The model characterizes the interaction between a hydrophilic AFM tip and a nanobubble at the last stage of tip approach when a thin film of liquid is trapped between the bubble surface and the tip apex, as sketched in Fig. 6b.[24]

The relation between the displacement ΔX of the tip apex and the interaction force F experienced by the tip is given by

$$\Delta X = \frac{F}{4\pi\gamma}\left\{\log\left(\frac{FR_{bt}}{8\pi\gamma R_c^{\,2}}\right) + 2B(\theta_{nano}) - \frac{4\pi\gamma}{k_{cant}} - 1\right\} \quad (1)$$

where k_{cant} is the stiffness of the cantilever, γ is the surface tension and the reduced radius R_{bt} is given by

$$R_{bt} \approx \left(\frac{1}{R_c} + \frac{1}{R_{tip}}\right)^{-1} \quad (2)$$

where R_c is the curvature of the bubble and R_{tip} is the radius of the tip apex. $B(\theta_{nano})$ is a parameter related to the constant volume constraint under the assumption that the bubble deforms with the constant contact angle θ_{nano}. It is described by eqn (3):

$$B(\theta_{nano}) = 1 + \frac{1}{2}\log\left(\frac{1+\cos\theta_{nano}}{1-\cos\theta_{nano}}\right) - \frac{1}{2+\cos\theta_{nano}}. \quad (3)$$

This formula is valid for high forces and for a small interaction zone and small deformations compared to the bubble size (radius of curvature). This constraint is satisfied for surface nanobubbles in our experiments. Moreover, the model assumes that the volume of the bubble is constant at all stages of interaction and the contact angle does not change. The initial separation used as an input parameter in the model was chosen as 17 nm and is equal to the unperturbed bubble height H_{bub} extracted from the force curve. The values of other parameters used in the model were as follows: tip radius $R_{tip} = 20$ nm, surface tension $\gamma = 0.07$ N m^{-1}, cantilever stiffness $k_{cant} = 0.05$ N m^{-1}. The forces calculated from the model formed a force curve shown in Fig. 6a.

The good agreement between the force curves from the model and from the experiment indicates that (1) the AFM tip used for the scanning was sharp and hydrophilic, (2) the interaction forces between the tip and the nanobubble in the AFM experiment had a hydrodynamic origin. This result means that a thin liquid film was present between the tip apex and the

bubble during the measurement. The increased repulsion measured on the bubble in the experiment originated from the squeezing of the film and the displacement of water from the shrinking space between the bubble surface and the approaching AFM tip.

The discrepancy in interaction strengths measured for the same bubble in lift mode and in FV AFM is the manifestation of a different nature of tip-bubble interaction in both AFM modes that is caused by different directions of tip movement. As shown in Fig. 1, during scanning in lift mode, the tip is moved horizontally so that it approaches the bubble only from the side. On the contrary, during the force measurement, the tip is displaced only in the vertical direction so that it approaches the bubble from the top. Because the geometry of the interaction, and the speed and direction of the tip movement differed in the lift mode and in the force measurement, the hydrodynamic effect and the cantilever response were different. Apparently, the bubble top resisted the squeezing of the liquid film by the tip more than the bubble side and the cantilever bent more upwards during the force measurement than during the scanning done in the lift mode.

An upward bending of the cantilever was measured only on the bubble near the bubble center. Near the edges of the bubble, the cantilever bent downwards both in the lift mode and in the FV mode. The local variations in the deflection signal with the spatial position of the tip over the bubble observed in the plots in Fig. 5 suggest different tip-bubble interactions near the bubble periphery as compared to the bubble center. Spatial variations of various parameters extracted from the force–distance curves or amplitude–distance curves were also reported in the experiments done in Peak Force AFM,[25,47,48] in FV AFM,[58] and in amplitude spectroscopy (Amplitude Volume) AFM.[46]

As shown in the plots in Fig. 5, the total spatial extent of non-zero cantilever deflection signal in the horizontal direction was larger in the lift mode than in the FV mode at a fixed tip-sample separation distance. In the lift mode, when the tip was approaching the bubble from the side, it started to bend downwards at the distance about 100 nm from the position of the estimated unperturbed bubble surface, so *before* the bubble. After passing through the bubble, the cantilever returned to the unbent position about 100 nm *after* the position of the unperturbed bubble surface. No analogous behavior was observed in the FV experiment. However, in the vertical direction, the spatial extent of non-zero deflection signal measured in FV was larger than in the lift mode. As shown in the plots in Fig. 5, in the FV mode, downward bending of the cantilever was measured over the bubble top for a tip-sample separation of 20 nm, whereas no interaction was measured in the lift mode for the lift height of 20 nm.

The difference in the spatial extent of the tip-bubble interaction measured in lift mode and in FV mode can again be explained by different tip movement in these two modes. In FV, the tip approached the bubble vertically from the top and hence the interaction region was extended in the vertical direction. The initial attraction that caused bending of the cantilever at the separations larger than the local bubble height H_{bub} is well visible in the force curve plotted in Fig. 6a. This effect could be caused by a jump of the bubble interface towards the tip. By contrast, in lift mode, the interaction region was extended in the horizontal direction because the tip was approaching the bubble from the side and the bubble interface moved sideways towards the tip. In both cases, the tip shape might also play a role and the interaction of the bubble surface with the tip apex was different from its interaction with the tip side.

We expect that the tip-bubble interaction and nanobubble deformation in TM AFM will be the resultant of the effects arising from the horizontal movement of the tip over the bubble and the simultaneous vertical movement due to cantilever oscillations.

The information on the deflection of the cantilever on surface nanobubbles available in the literature is consistent with our results. Janda *et al.* studied nanobubbles in aqueous solution on graphite in modified AFM dynamic force mode.[26] Deflection measurements were done simultaneously with topographic imaging and the deflection was measured at zero tip-sample separation. The deflection signal was nearly zero on the substrate and negative on all nanobubbles. The bubbles' footprints in the deflection image had approximately the same widths as the widths of the corresponding bubbles in the topographic image. Zhang *et al.*[49] conducted a series of measurements in lift mode AFM on nanobubbles on octadecyltrichlorosilane (OTS) modified silicon substrates in ~0.5 CMC Tween 20 solution, and obtained results comparable to ours. In the experiment, the bubble height and width estimated from TM height image were 44 nm and 375 nm, respectively. The deflection on the bubble was measured at lift heights varied between 10 and 160 nm. In all lift mode images, the deflection on the bubble was different from the deflection measured on the substrate. It changed from the positive values all over the bubble for low lift heights to negative values for increased lift heights (the switch from positive to negative took place between 20 and 40 nm lift height). At 10 nm lift height, the area of the bubble visible in the image was slightly smaller than the area of the bubble base in the TM height image. Then, the apparent bubble area decreased for the lift heights increased from 10 nm to 40 nm. With a further lift height increase up to 160 nm, the footprint area stayed approximately constant and the deflection became weaker until 160 nm, when the bubble disappeared completely from the image. No information about the strength of the interaction and a magnitude of deflection was provided. In the view of our findings, the results of Zhang *et al.* showing non-zero deflection signal detected far above the estimated bubble height indicate the presence of a strong attractive interaction between the tip and the bubble. Our suggestion is in line with the authors' conclusion drawn in their report that the surfactant solution made nanobubbles more pliable. Therefore, it was possible that the bubble in the lift mode experiment was stretched upwards toward the tip far above its regular height.

In our experiment, no forces were detected at tip-sample separation distances exceeding the bubble height by 80 nm. We conclude that *no* flow was present anywhere above or around the bubble up to at least 120 nm. Our finding is in line with the

results reported by other authors, and obtained using various techniques.[23,59]

The generalization of our findings to other systems including soft organic or polymeric clusters or (ultra)small droplets *etc.* appears to us very relevant. Unfortunately, the physics is for the following reasons system-dependent and it seems that a generalization may only work for standardized systems:

(a) tapping mode AFM is dominated by energy dissipation, which is system-dependent, primarily depending on relaxation channels and characteristic times, among others;

(b) intermolecular forces that govern attraction and repulsion depend on the medium as well as on the particular molecules and their arrangement;

(c) the tip shape in 3D determines the range of interaction forces and the local contact geometry; this varies with each tip and should be explicitly considered;

(d) AFM tip functionality (*e.g.* by functionalization with monolayers) may possess an effect on (a) and (b) and hence need to be considered separately.

Although a complete description of these factors for random systems may be not feasible, it should be in reach for well-defined systems.

5 Conclusions

Based on the results of our combined AFM TM, lift mode and FV measurements of argon nanobubbles on HOPG in water, we have shown that the interaction between the AFM tip and the surface nanobubble was weak and limited to the volume occupied by the bubble and to its closest vicinity. No interaction with the liquid above or around the bubble surface was detected. The strength and the character (repulsive or attractive) of the interaction depended on the vertical and horizontal position of the tip over the bubble. Attractive forces dominated the region near the bubble rim, whereas repulsive (or less attractive) forces dominated the region near the bubble center. The appearance of the bubble in the lift mode deflection images varied depending on the shape of the individual force–distance curves, and on the bubble size.

Good agreement between the results of the experiment and of the dynamic interaction model indicated that the AFM tip was hydrophilic and interacted with nanobubbles through a thin film of liquid. The hydrodynamic effect arising from squeezing the thin film during the measurements played a role in the interaction and influenced the cantilever response during the scanning. Its strength and spatial extent were closely related to the character and direction of the tip movement during the scanning. In lift mode, the tip approached the nanobubble only from the side and the hydrodynamic repulsion was less pronounced so that only a weak interaction between the tip and the bubble was measured. In the FV mode, the tip approached the bubble only from the top, and the hydrodynamic effect and measured repulsion were stronger.

Finally, we have shown that the nanobubble appearance in the AFM images not only depends on the tip shape and cleanness, and the scanning parameters chosen, but also is sensitive to the measuring conditions related to the scanning mode utilized in the AFM experiment. Because the hydrodynamic effect is related to the bubble deformation, its possible consequences for the measurements of nanobubble dimension must be taken into account, especially when measuring nanobubbles in the AFM scanning modes that involve complex tip movement.

Acknowledgements

The authors would like to thank Dr S. Druzhinin and Dr H. Kneppe for enlightening discussions and helpful suggestions and gratefully acknowledge financial support from the Deutsche Forschungsgemeinschaft (DFG grant no. INST 221/87-1 FUGG), the European Research Council (ERC grant to HS, ERC grant agreement no. 279202) and the University of Siegen.

Notes and references

1 J. N. Israelachvili and R. M. Pashley, *Nature*, 1982, **300**, 341.
2 H. K. Christenson and P. M. Claesson, *Science*, 1988, **239**, 390.
3 J. L. Parker, P. M. Claesson and P. Attard, *J. Phys. Chem.*, 1994, **98**, 8468.
4 K. W. Stockelhuber, B. Radoev, A. Wenger and H. J. Schulze, *Langmuir*, 2004, **20**, 164.
5 Z. Wu, X. Zhang, X. Zhang, J. Sun, Y. Dong and J. Hu, *Chin. Sci. Bull.*, 2007, **52**, 1913.
6 A. Maali and B. Bhushan, *J. Phys.: Condens. Matter*, 2013, **25**, 184003.
7 Y. Wei, S. Brandl, F. Goodwin and D. Back, *Future Fab. Intl.*, 2007, **22**, 65.
8 H. Schubert, *Int. J. Miner. Process.*, 2005, **78**, 11.
9 G. Liu and V. S. J. Craig, *ACS Appl. Mater. Interfaces*, 2009, **1**, 481.
10 S. Yang and A. Dusterwinkel, *Langmuir*, 2011, **27**, 11430.
11 N. Ishida, T. Inoue, M. Miyahara and K. Higashitani, *Langmuir*, 2000, **16**, 6377.
12 S. T. Lou, Z. Q. Ouyang, Y. Zhang, X. J. Li, J. Hu, M. Q. Li and F. J. Yang, *J. Vac. Sci. Technol., B: Microelectron. Nanometer Struct.*, 2000, **18**, 2573.
13 J. W. G. Tyrrell and P. Attard, *Phys. Rev. Lett.*, 2001, **87**, 1761041.
14 R. Steitz, T. Gutberlet, T. Hauss, B. Klösgen, R. Krastev, S. Schemmel, A. C. Simonsen and G. H. Findenegg, *Langmuir*, 2003, **19**, 2409.
15 X. H. Zhang, A. Quinn and W. A. Ducker, *Langmuir*, 2008, **24**, 4756.
16 M. Switkes and J. W. Ruberti, *Appl. Phys. Lett.*, 2007, **84**, 4759.
17 J. Yang, J. Duan, D. Fornasiero and J. Ralston, *Phys. Chem. Chem. Phys.*, 2007, **9**, 6327.
18 T. R. Jensen, M. O. Jensen, N. Reitzel, K. Balashev, G. H. Peters, K. Kjaer and T. Bjørnholm, *Phys. Rev. Lett.*, 2003, **90**, 086101.
19 M. A. Mezger, S. A. B. Schöder, H. A. Reichert, H. A. Schröder, J. A. Okasinski, V. B. Honkimäki, J. C. Ralston, J. D. Bilgram, R. A. E. Roth and H. Dosch, *J. Chem. Phys.*, 2008, **128**, 244705.

20 L. Zhang, B. Zhao, L. Xue, Z. Guo, Y. Dong, H. Fang, R. Tai and J. Hu, *J. Synchrotron Radiat.*, 2013, **20**, 413.
21 S. Karpitschka, E. Dietrich, J. R. T. Seddon, H. J. W. Zandvliet, D. Lohse and H. Riegler, *Phys. Rev. Lett.*, 2012, **109**, 066102.
22 U. Mirsaidov, C.-D. Ohl and P. Matsudaira, *Soft Matter*, 2012, **8**, 3108.
23 C. U. Chan and C.-D. Ohl, *Phys. Rev. Lett.*, 2012, **109**, 174501.
24 W. Walczyk and H. Schönherr, *Langmuir*, 2014, 7112–7126.
25 B. Zhao, Y. Song, S. Wang, B. Dai, L. Zhang, Y. Dong, J. Lü and J. Hu, *Soft Matter*, 2013, **9**, 8837.
26 P. Janda, O. Frank, Z. Bastl, M Klementová, H. Tarábková and L. Kavan, *Nanotechnology*, 2010, **21**, 95707.
27 X. Zhang, D. Y. C. Chan, D. Wang and N. Maeda, *Langmuir*, 2013, **29**, 1017.
28 J. R. T. Seddon and D. Lohse, *J. Phys.: Condens. Matter*, 2011, **23**, 133001.
29 V. S. J. Craig, *Soft Matter*, 2011, **7**, 40.
30 B. Song, W. Walczyk and H. Schönherr, *Langmuir*, 2011, **27**, 8223.
31 W. A. Ducker, *Langmuir*, 2009, **25**, 8907.
32 S. Wang, M. Liu and Y. Dong, *J. Phys.: Condens. Matter*, 2013, **25**, 184007.
33 Y. Liu and X. Zhang, *J. Chem. Phys.*, 2013, **138**, 014706.
34 M. P. Brenner and D. Lohse, *Phys. Rev. Lett.*, 2008, **101**, 214505.
35 J. R. T. Seddon, H. J. W. Zandvliet and D. Lohse, *Phys. Rev. Lett.*, 2011, **107**, 116101.
36 N. D. Petsev, M. S. Shell and L. G. Leal, *Phys. Rev. Lett. E*, 2013, **88**, 10402.
37 J. H. Weijs and D. Lohse, *Phys. Rev. Lett.*, 2013, **110**, 054501.
38 J. R. T. Seddon, E. S. Kooij, B. Poelsema, J. W. Zandvliet and D. Lohse, *Phys. Rev. Lett.*, 2011, **106**, 056101.
39 P. Grosfils, *J. Phys.: Condens. Matter*, 2013, **25**, 184006.
40 R. P. Berkelaar, H. J. W. Zandvliet and D. Lohse, *Langmuir*, 2013, **29**, 11337.
41 M. Mazdumer and B. Bhushan, *Soft Matter*, 2011, **7**, 9184.
42 A. L. Weisenhorn, M. Khirsandi, S. Kasas, V. Gotzos and H.-J. Butt, *Nanotechnology*, 1993, **4**, 106.
43 W. Walczyk and H. Schönherr, *Langmuir*, 2013, **29**, 620.
44 B. M. Borkent, S. de Beer, F. Mugele and D. Lohse, *Langmuir*, 2010, **26**, 260.
45 S. Yang, E. S. Kooij, B. Poelsema, D. Lohse and H. J. W. Zandvliet, *EPL*, 2008, **81**, 64006.
46 B. Bhushan, Y. Wang and A. Maali, *J. Phys.: Condens. Matter*, 2008, **20**, 485004.
47 C. W. Yang, Y. H. Lu and I. S. Hwang, *J. Phys.: Condens. Matter*, 2013, **25**, 184010.
48 W. Walczyk, P. M. Schön and H. Schönherr, *J. Phys.: Condens. Matter*, 2013, **25**, 184005.
49 X. H. Zhang, N. Maeda and V. S. J. Craig, *Langmuir*, 2006, **22**, 5025.
50 M. Holmberg, A. Kühle, J. Garnæs, K. A. Mørch and A. Boisen, *Langmuir*, 2003, **19**, 10510.
51 A. Agrawal, J. Park, D. Y. Ryu, P. T. Hammond, T. P. Russel and G. H. McKinley, *Nano Lett.*, 2005, **5**, 1751.
52 Y. H. Lu, C. W. Yang and I. S. Hwang, *Langmuir*, 2012, **28**, 12691.
53 H. Peng, P. A. Hampton and A. V. Nguyen, *Langmuir*, 2013, **29**, 6123.
54 J. Ally, M. Kappl, H.-J. Butt and A. Amirfazli, *Langmuir*, 2010, **26**, 18135.
55 D. Y. C. Chan, R. R. Dagastine and L. R. White, *J. Colloid Interface Sci.*, 2001, **236**, 141.
56 R. R. Dagastine and L. R. White, *J. Colloid Interface Sci.*, 2002, **247**, 310.
57 R. F. Tabor, F. Grieser, R. R. Dagastine and D. Y. C. Chan, *J. Colloid Interface Sci.*, 2012, **371**, 1.
58 W. Walczyk and H. Schönherr, manuscript submitted.
59 E. Dietrich, H. J. W. Zandvliet, D. Lohse and J. R. T. Seddon, *J. Phys.: Condens. Matter*, 2013, **25**, 184009.